Available online at www.sciencedirect.com
SCIENCE DIRECT®
Catalysis Today 100 (2005) 261–267
CATALYSIS TODAY
www.elsevier.com/locate/cattod

Effect of catalyst preparation on the carbon nanotube growth rate

Zhixin Yu [a], De Chen [a], Bård Tøtdal [b], Anders Holmen [a,*]

[a] Department of Chemical Engineering, Norwegian University of Science and Technology (NTNU), N-7491 Trondheim, Norway
[b] Department of Physics, Norwegian University of Science and Technology (NTNU), N-7491 Trondheim, Norway

Abstract

A series of silica supported Fe catalysts were prepared by different methods in order to obtain varying Fe particle sizes. The catalysts were characterized by XRD, TPR, BET, and TEM. The CNT growth from CO disproportionation was studied in order to establish a relationship between the CNT growth rate and the particle size. We found that there is an optimum catalyst particle size at around 13–15 nm which will lead to the maximum growth rate. The influence of the metal loading on the growth rate was also investigated. A CNT growth model has been formulated to explain the experimental results.

Keywords: Fe catalyst; Particle size; Growth rate; Metal loading; Growth model

1. Introduction

The properties of carbon nanotubes (CNTs) have brought about an enormous interest to this new form of carbon, which presents high expectations for applications in various fields. In spite of the great progress in the synthesis, one of the key problems still persists, that is, the availability of large quantities of CNTs with well defined structures. The most promising way for large scale CNT synthesis is chemical vapor deposition (CVD). In the CVD process, the CNT growth rate and productivity are important economical issues, which have generally been optimized with regard to synthesis conditions or catalyst composition.

Recently it has been noticed that the catalyst particle size is an important factor in CNT growth and catalysts with large particle sizes have been claimed ineffective [1–3]. Indeed, it has been shown decades ago both experimentally and theoretically that the carbon filament growth rate increases with decreasing catalyst particle size [4,5]. However, previous studies have been limited to relatively large particles (>20 nm), and the growth rate has been expressed as the length increase of the filaments. It will therefore be of interest to further study the dependence of the global growth rate on the catalyst particle size with smaller dimensions. Small catalyst particles are also more interesting because they produce CNTs with smaller diameters, which are normally desired.

A crucial point is to control the synthesis of metal particles with desired sizes that are stable at the high temperatures required for the CNT formation. Precise control of the catalyst particle size depends on the art of nanotechnology, which usually involves surfactant assisted growth [6]. To provide the active catalyst with the desired thermal stability, a support is generally utilized. Nevertheless, it is difficult to introduce the prepared nanoparticles to a suitable catalyst support in a bulk system.

In this study we prepared several Fe catalysts supported on silica (Fe/SiO_2) by different methods in order to obtain a wide range of sizes of the iron particles. It is expected that a size distribution will be present in such bulk catalysts. The main purpose of the study is to reveal the dependence of the growth rate on the catalyst particle size. Attempt was also made to increase the growth rate by increasing the metal loading of the catalyst.

2. Experimental

2.1. Preparation and characterization of the catalysts

The methods and precursors used in preparing the catalysts are summarized in Table 1. The metal loading is

* Corresponding author. Tel.: +47 73594151; fax: +47 73595047.
E-mail address: holmen@chemeng.ntnu.no (A. Holmen).

0920-5861/$ – see front matter © 2004 Elsevier B.V. All rights reserved.
doi:10.1016/j.cattod.2004.09.060

Table 1
Precursors, properties, and productivity of different catalysts

Catalysts	Precursors[a]	Phases[b]	D_{Fe} (nm)	Reduced (%)[c]	Reduced (%)[d]	BET (m^2/g)	Productivity (g_C/g_{Cat})[e]
UREA	$FeCl_2$, urea	Fe_2SiO_4, Fe	11	59.8	81.2	188.93	2.64
CYA	$FeCl_2$, $Na_2Fe(CN)_5NO$	Fe	30	53.7	55.5	91.19	0.23
NH_3	$Fe(NO_3)_3$, NH_4OH	Fe_2SiO_4, Fe	18	54.0	89.8	131.51	
IMP	$Fe(NO_3)_3$	Fe	15	64.8	91.0	84.25	
S–G (N)	TEOS, $Fe(NO_3)_3$	Fe_2SiO_4, Fe	21	63.5	80.2	378.33	
S–G (CA)	TEOS, $Fe(NO_3)_3$, $C_6H_8O_7$	Fe_2SiO_4, Fe	5	70.9	89.4	438.71	
UREA-40	$FeCl_2$, urea	Fe_2SiO_4, Fe	18			337.50	6.40
UREA-60	$FeCl_2$, urea	Fe	28				14.97
CYA-40	$FeCl_2$, $Na_2Fe(CN)_5NO$	Fe	36			15.65	0.56
CYA-60	$FeCl_2$, $Na_2Fe(CN)_5NO$	Fe	37				9.98

[a] Except the S–G catalysts, all others use silica powder (Degussa Aerosil 200) as catalyst support.
[b] Phases in the reduced state.
[c] Percentage reduced when temperature reaches 1000 °C.
[d] Percentage reduced after isothermal reduction at 1000 °C for 1 h.
[e] Values based on 9 h synthesis time.

20 wt.% Fe on silica in the reduced state, unless otherwise stated.

Deposition–precipitation (D–P) by urea hydrolysis (denoted as UREA) was prepared from silica and $FeCl_2$ [7,8]. Catalysts with metal loadings of 40% and 60% were also prepared and denoted as UREA-40 and UREA-60. For D–P from cyanide precursor (denoted as CYA) [9], $Na_2Fe(CN)_5NO$ was used to precipitate $FeCl_2$ in the silica suspension. Catalysts with 40% and 60% loading are denoted as CYA-40 and CYA-60. One catalyst was prepared from $Fe(NO_3)_3$ and NH_4OH (denoted as NH_3), in a way similar to the CYA catalyst. For impregnation (denoted as IMP), a two-step incipient wetness method was employed. In the sol–gel process [10], catalysts with citric acid (denoted as S–G (CA)), or without citric acid (denoted as S–G (N)) were prepared. The detailed preparation procedures are described in the literature cited above [7–10]. All catalysts were calcined at 600 °C in air.

2.2. CNT growth

The CNT synthesis was performed in a vertical quartz reactor. For a given reaction, the catalysts were reduced in 100 ml/min H_2/He (25 vol.%) at 600 °C for 6 h. Subsequently, synthesis gas (CO/H_2 = 40:10 ml/min) was introduced, and the reaction was carried out for 9.5 h at 600 °C and 6.5 h at 650 °C. The gaseous products were monitored with an online gas chromatograph (GC).

2.3. Catalyst and CNT characterization

An X-ray diffraction (XRD) study was performed using a Siemens D5005 X-ray diffractometer. The particle size is calculated by the Scherrer equation, assuming K factor 0.89. For the XRD study of the reduced catalysts, iron oxides were reduced for 6 h at 600 °C and then passivated. Temperature programmed reduction (TPR) was carried out using a Perkin-Elmer thermogravimetric analyzer (TGA). TPR was performed in 80 ml/min H_2/Ar mixture (7 vol.%) at a heating rate of 5 °C/min from 40 to 1000 °C, then maintained at 1000 °C for 1 h. BET study was carried out using Micromeritics TRiStar 3000. Transmission electron microscopy (TEM) investigation was performed using a JEOL 2010F electron microscope.

3. Results and discussion

3.1. Catalyst preparation and characterization

3.1.1. XRD study

After calcination, the iron oxide containing catalysts exhibit two different colours. The colour of the CYA and IMP catalyst is dark orange. While for all the other catalysts, the colour is close to dark brown. Fig. 1(a) shows the XRD profiles of the calcined catalysts. For the UREA, NH_3, S–G (CA) catalysts, the diffraction only gives weak and broad bands of silica and iron oxide, which is centred at around 22, 35 and 62° (top). This fact indicates that iron oxide is highly dispersed in the silica matrix and of small particle size. It is not possible to confirm the existence of silicate species from those broad peaks. The curve in the middle is the diffraction pattern of S–G (N), which exhibits slightly more intense peaks of iron oxide. While for the CYA and IMP catalyst, the diffraction pattern gives single phase of Fe_2O_3 with very strong diffractions. This might suggest that the particle size of iron oxide is the largest for those two catalysts.

After reduction, the diffraction pattern of UREA, NH_3, S–G (N), S–G (CA) catalysts are similar, which is represented by the diffractogram on the top of Fig. 1(b). Those catalysts exhibit strong diffractions of both Fe and Fe_2SiO_4. The formation of iron silicate could be induced during either calcination or reduction of iron oxides, and suggests strong metal–support interaction in the catalyst [11]. The diffractogram in the bottom of Fig. 1(b) is characteristic of the CYA and IMP catalysts. It displays

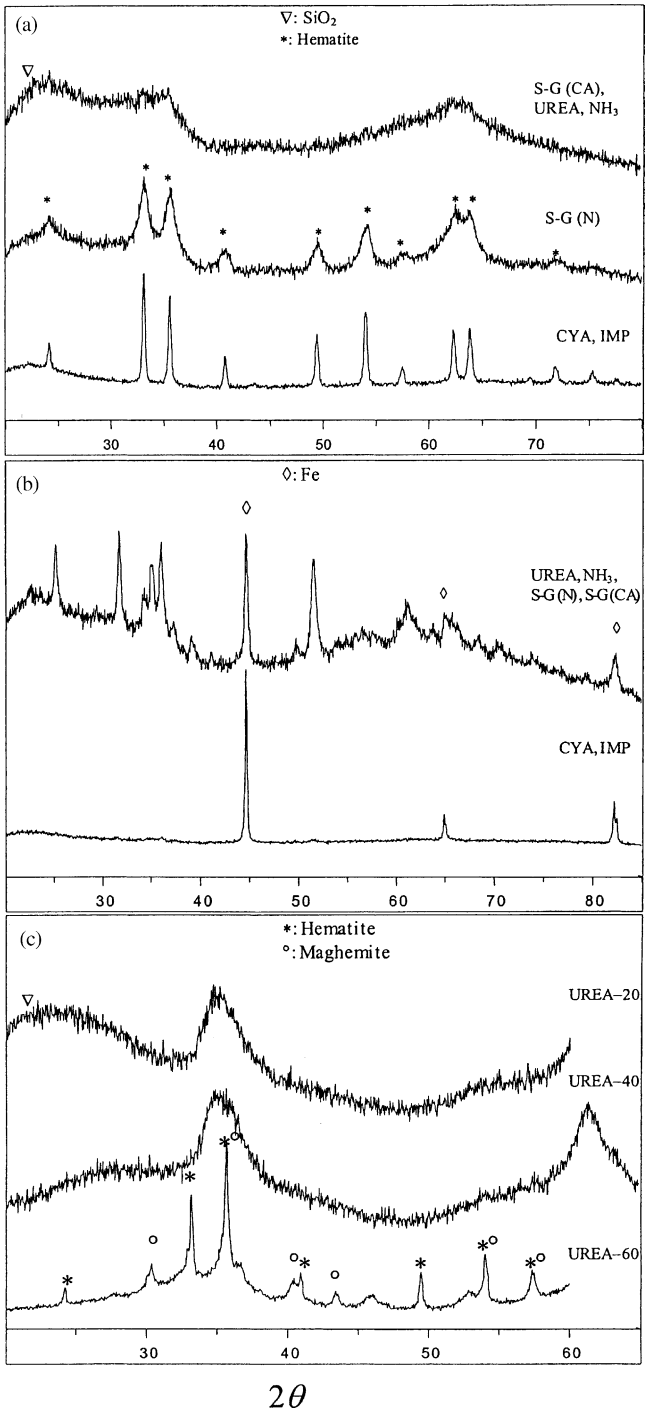

Fig. 1. XRD diffraction patterns of the catalysts prepared by different methods: (a) calcined catalysts; (b) reduced catalysts; (c) calcined UREA catalysts with different metal loadings. In (b) all other peaks except those of Fe are ascribed to Fe_2SiO_4.

strong reflections of Fe, though for the IMP catalyst very weak peaks of Fe_2SiO_4 are also detected. It is attempting to correlate the colour of the iron oxide with Fe_2SiO_4 formation. Dark orange is associated with the CYA and IMP catalyst, which has no Fe_2SiO_4 in their reduced state. On the contrary, when Fe_2SiO_4 is formed, the colour of the calcined samples is always close to dark brown.

Scherrer equation calculation gives that different preparation methods lead to varying mean particle size of the reduced samples (Table 1), ranging from 5 to 30 nm. The particle size follows the sequence S–G (CA) < UREA < IMP < NH_3 < S–G (N) < CYA. The reduced catalysts are responsible for the CNT growth. It is therefore the size of the reduced particles that is pertinent for comparing the growth rate.

The motivation for using different catalyst preparation methods is to obtain a wide range of particle sizes. However, it is extremely difficult to vary systematically the size of the active particles while maintaining a narrow size distribution. Normal precipitation will lead to local supersaturation and inhomogeneous distribution, so we performed all precipitation by deposition–precipitation [8]. Urea hydrolysis generates a very homogeneous medium for precipitation, hence it produces relatively small particles. The precipitation of Fe(III) is rather complicated and difficult to control [11], therefore the NH_3 catalyst results in larger sizes. The largest particles are from the CYA catalyst, which suppresses metal–support interaction [9], thus leading to the largest size and size distribution. It can be concluded that different particle sizes are controlled by the precipitation rate, degree of supersaturation, and extent of metal–support interaction. The S–G (CA) has the smallest particle sizes of 5 nm, and sol–gel methods are well known to produce catalysts with small particles and highly homogeneous distribution of metal in the support [10,12].

Fig. 1(c) shows the diffractograms of the calcined UREA, UREA-40, UREA-60 catalysts. It is clear that when the loading increases to 40%, the iron oxides still exhibit only weak and broad bands, just like the 20% catalyst, suggesting good dispersion and small size. The intense signal for the UREA-60 catalyst, however, suggests the presence of large iron oxide particles. Indeed, there are two different types of Fe_2O_3 formed, namely hematite and maghemite. Therefore, for a high loading of 60% the UREA catalyst achieves neither a homogeneous distribution nor the single phase. The XRD profile (not shown) of the reduced sample displays that the UREA and UREA-40 catalysts present diffraction peaks of both Fe_2SiO_4 and Fe. While for the UREA-60 catalyst, well-defined peaks of Fe appear without detectable reflections from Fe_2SiO_4. The Scherrer equation shows that the particle size increased slightly to 18 nm for UREA-40, but increased to 28 nm for the UREA-60 catalyst. The XRD patterns of the CYA-40 and CYA-60 show no difference from that of the CYA catalyst, for both the calcined and reduced samples. The Fe particle sizes are 36 and 37 nm, respectively (Table 1).

3.1.2. TPR study

The differential thermogravimetric (DTG) curve (Fig. 2) displays the reduction profile of the catalysts, listed according to their particle sizes. The catalysts undergo successive transformations during TPR treatment, including the loss of water, $Fe_2O_3 \rightarrow Fe_3O_4$, $Fe_3O_4 \rightarrow FeO$, and

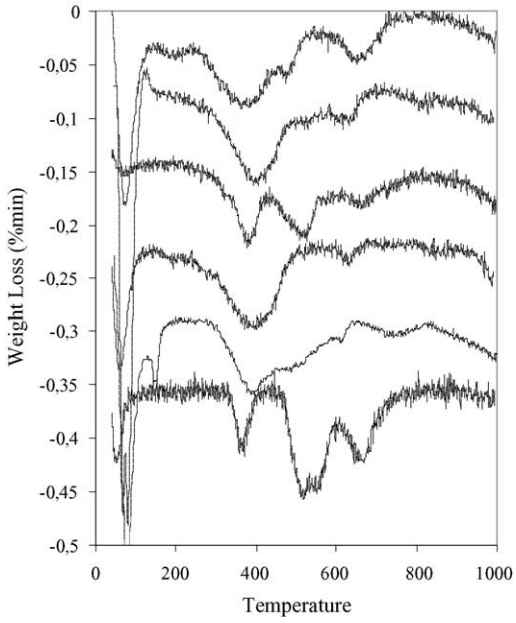

Fig. 2. TPR profiles of the catalysts from top: S–G (CA), UREA, IMP, NH_3, S–G (N), CYA.

FeO → Fe. The four main peaks of the rate of weight loss occurred at about 100, 400, 500–600, and 650–850 °C. The continuous weight loss at 1000 °C can be ascribed to the reduction of silicate species [13].

It has been reported that the reduction of Fe_2O_3 to Fe_3O_4 normally occurs at around 400 °C [14], which agrees well with the TPR curves in Fig. 2. Therefore, the weight loss at temperatures lower than 200 °C is ascribed solely to the loss of water. This is reasonable because all the DTG curves normally display zero weight loss in the temperature range of 150–250 °C. For a 20% loading catalyst, a theoretical value 7.91% of weight loss is expected if the Fe species are completely reduced. Based on this theoretical value, the percentage of Fe that is reduced when the reduction temperature reaches 1000 °C and after isothermal reduction at 1000 °C can be calculated (Table 1). It was found that 54–71% reduction is completed during the first stage, and 56–91% reduction is completed after the isothermal period. Such a discrepancy indicates that a minor portion of iron always remains in the unreduced state, which has been frequently reported [12,13]. In addition, it was found that the reduction peaks for the IMP, CYA, and S–G (CA) catalysts are at a relatively lower temperature region than the other catalysts. For the UREA, NH_3, S–G (N) catalysts, it is probably that the formation of Fe_2SiO_4 induces strong metal-support interaction that retarded the reduction processes. It is not clear why the S–G (CA) catalyst is also reduced at lower temperature because Fe_2SiO_4 is present in this catalyst.

3.1.3. BET measurement

The surface area of the original silica support was determined to be 200 m^2/g. BET measurements reveal that introducing the metal precursors onto the support reduced the surface area of all catalysts. The IMP and CYA catalysts have the smallest surface area lower than 100 m^2/g, while the catalysts prepared from sol–gel method have surface area as high as 400 m^2/g. BET measurements confirmed that those catalysts containing Fe_2SiO_4 have relatively larger surface areas than those without Fe_2SiO_4, in agreement with earlier studies [11]. Interestingly, the further increase of metal loading increased the surface area of the UREA-40 catalyst, while it decreased the surface area of the CYA-40 catalyst.

3.1.4. TEM characterization

TEM provides a useful visual method to analyze the morphology and the particle size of the catalysts, but it provides information limited to a small part of the sample. On the contrary, XRD is a volume-average technique, which is more appropriate to characterize the average size of the bulk catalyst. TEM pictures of the catalysts were recorded with the smallest (S–G (CA)) and largest particle size (CYA) to confirm the XRD results. Fig. 3(a) is a high resolution TEM image of the S–G (CA) catalyst. It is evident that the Fe particles (black dots) are dispersed homogeneously in the silica matrix (white). The Fe particles are surrounded evenly by silica, which should be beneficial for preventing sintering during carbon growth. The particle size averaged from 120 particles gives a value of 6 nm, in accordance with the XRD study. On the contrary, in the reduced CYA catalyst the particles are not always homogeneous (Fig. 3(b)). Though most of the Fe particles have spherical shape and diameters around 30 nm, very large particles with different shapes can be observed.

3.2. CNT growth

3.2.1. Effect of particle size

The kinetic behaviour calculated from GC analysis is quite similar for all the catalysts: the catalysts undergo very slow but continuous deactivation in the process. The growth rate at 650 °C is either close to, or lower than that at 600 °C. The rates are calculated based on 6.5 h synthesis time.

The dependence of carbon growth rate on Fe particle sizes at two different temperatures is displayed in Fig. 4(a). For the catalyst with the largest particle size (CYA, D_{Fe} = 30 nm), the growth rate is at a minimum of 0.03 g_C/g_{Cat} h. When the particle size decreases, the rate increases sharply. It reaches a maximum over the IMP catalyst with a particle size of 15 nm. When the particle size is decreased further, however, the growth rate declines. With the smallest particles of 5 nm, the growth rate is also very low. Exactly the same trend is obtained at 650 °C, though the dependence of the growth rate on particle size is levelled off, in agreement with the results from Baker et al. [4]. Based on these results the optimum particle size lies at about 13–15 nm at both temperatures.

As stated before, all the catalysts are not completely reduced at 600 °C and silicate species are always present in some proportion. The corresponding reduced catalysts

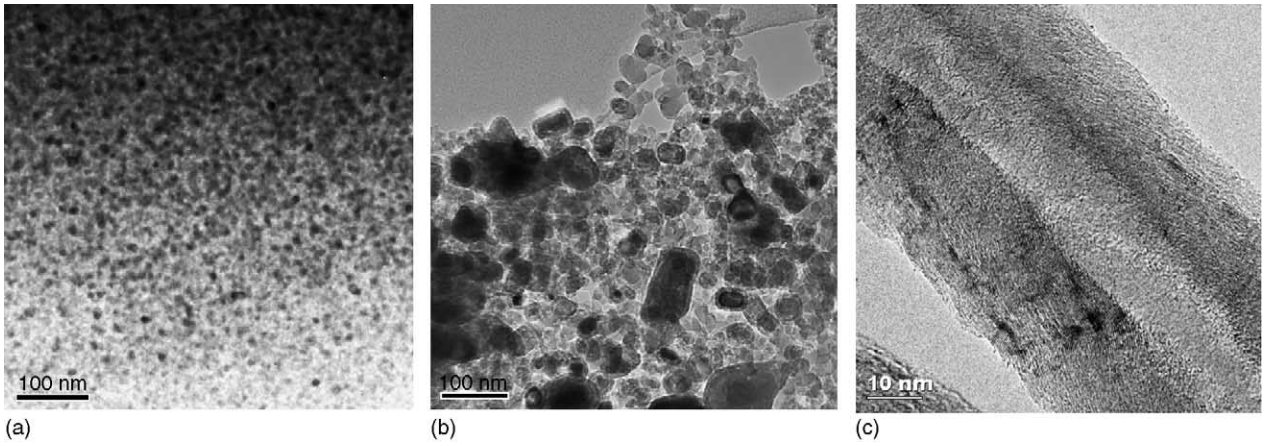

Fig. 3. TEM images of: (a) the reduced S–G (CA) catalyst showing the small size and narrow size distribution of this catalyst; (b) the reduced CYA catalyst showing inhomogeneous particles; (c) CNTs grown on the CYA catalyst at 600 °C showing graphite planes inclined at a small angle to the tube axis.

contain silicate species in different amounts which will influence the formation of carbon filaments [13]. Baker et al. [15] assumed that Fe_2SiO_4 formed by the interaction of Fe with silica decreased the carbon solubility and lowered the rate of carbon diffusion through the catalytic particle.

A more accurate comparison and determination of rate-size dependence should take this effect into consideration. The reducibility from TPR is a good indication of the active Fe species in the catalysts, because the reduction and the CNT growth were performed at exactly the same conditions over all the Fe/SiO_2 catalysts. From Table 1 it can be seen that the percentage reduced after both steps has no large difference among different catalysts. So even if the growth rate is normalized with respect to the percentage reduced, the overall trend of the rate-size dependence will not be changed at all. Hence, the size effect should be dominating over the effect of Fe_2SiO_4 formation.

The S–G (CA) catalyst has both a very small particle size and an extremely high surface area. However, it does not achieve a high production rate. In this regard it is also reasonable to conclude that the size effect is dominating over the effect of the surface area.

3.2.2. *Effect of metal loading*

Fig. 4(b) displays the growth curve for the series of UREA catalysts, and the productivity during 9 h synthesis time is summarized in Table 1. It is evident that an increase of the metal loading increased the growth rate significantly, though not with a linear relationship. For the cyanide catalysts, the catalysts did not lead to significant carbon growth at 20% and 40% loading (Table 1). However, when the loading was increased to 60%, the productivity increased sharply though still lower than the corresponding UREA-60 catalyst. The maximum growth rate was 1.66 g_C/g_{Cat} h, achieved over the UREA-60 catalyst.

The very low activity of CYA and CYA-40 catalysts can again be attributed to the large particle sizes. For the CYA-60 catalyst, we assume that the reason for the high activity at 60% metal loading is a very wide particle size distribution. The catalyst might have substantial amount of small particles, which could be responsible for the CNT growth on this catalyst. Similar to the UREA-60 catalyst, two different Fe_2O_3 phases might be present (Fig. 1(c)). The effect of two phase formation can not be simply excluded.

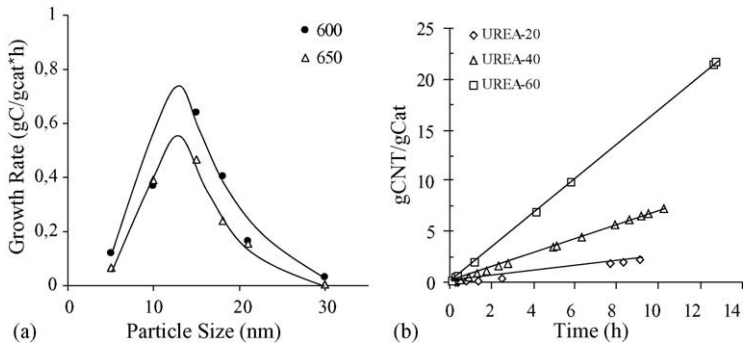

Fig. 4. (a) Dependence of growth rate on the particle sizes at 600 and 650 °C; (b) the CNT growth over the UREA catalysts with different metal loadings at 600 °C.

3.2.3. TEM characterization

The structure of the synthesized CNTs is not the focus of this study. One representative TEM image of the CNTs grown at 600 °C on the CYA catalyst from CO/H_2 (40:10) mixture is presented in Fig. 3(c). This high resolution TEM image clearly displays a tubular structure, with the graphite planes inclined at a very small angle to the tube axis. The CNTs synthesized from this series of iron catalysts probably have similar structures but different diameters.

3.3. CNT growth model

The size effect can be explained semi-quantitatively by a mathematical model, which is developed by considering the detailed surface reactions and growth mechanism of carbon filaments [16]. For catalytic growth of CNTs, it is accepted that a filament formed when carbon first deposited from the gas phase on one side of a catalyst particle and then diffused through the catalyst bulk, and finally precipitated at the other side of the catalyst particle. The diffusion of carbon through the particle is generally considered as the rate-determining step.

Regarding CO disproportionation to produce CNT in the presence of H_2, the following steps are involved:

Surface reaction:

$$CO + {}^* = CO^* \quad (1)$$

$$CO^* + {}^* = C^* + O^* \quad (2)$$

$$H_2 + 2^* = 2H^* \quad (3)$$

$$O^* + 2H^* = H_2O + 3^* \quad (4)$$

$$O^* + CO = CO_2 + {}^* \quad (5)$$

$$3Fe + C^* = Fe_3C + {}^* \quad (6)$$

Dissolution/segregation:

$$C^* = C_{Fe,f} + {}^* \quad (7)$$

Diffusion of carbon through iron:

$$C_{Fe,f} \rightarrow C_{Fe,r} \quad (8)$$

Precipitation/dissolution of carbon:

$$C_{Fe,r} = C_f \quad (9)$$

where $C_{Fe,\,f}$ is carbon dissolved in iron at the front side of the particle, which can be in the form of Fe_3C, and $C_{Fe,\,r}$ is carbon dissolved at the rear of the particle (support side).

At steady-state, the filament growth rate is directly proportional to the driving force of the carbon diffusion, which is the concentration gradient from one side of the particle to the other. The steady-state equation of continuity is therefore:

$$D \cdot \nabla^2(C) = 0 \quad (10)$$

The solution to Eq. (10) will give the carbon concentration as a function of position within the catalyst particle. The different mechanistic models would require different boundary conditions and values for the diffusion coefficient D. Thus the flux of carbon across either the leading face or the rear face could be evaluated.

For the present purpose a much simplified model will be used. It assumes that there is an effective diffusion path length, such that the carbon concentration gradient from the front of the particle to the rear of the particle can be approximated as the difference between carbon concentrations at these two locations divided by the diffusion path length. In that case the rate of carbon diffusion and thus the CNT growth rate, can be represented by: [17,18]

$$r = \frac{D_C}{d_{Fe}} a_{Fe}(C_{C-Fe,f} - C_{C-Fe,r}) \quad (11)$$

where r is CNT growth rate, D_C the effective carbon diffusivity, a_{Fe} the specific surface area of Fe, d_{Fe} the effective diffusion length, $C_{C-Fe,\,f}$ the carbon concentration at the gas side, and $C_{C-Fe,r}$ the carbon concentration at the rear side of the catalyst particle.

Assuming that segregation of carbon is a fast process, $C_{C-Fe,f}$ will be in equilibrium with surface carbon, which is determined by surface reactions. Provided that precipitation is a fast step, the carbon in bulk Fe at the rear side is in equilibrium with CNT, and $C_{C-Fe,r}$ is therefore identical with the saturation concentration of CNT (C_{sat}). It has been calculated numerically that the smaller the CNF diameter, the higher the saturation concentration of CNF [18].

From Eq. (11) the size effect can be explained nicely. A small crystal size of Fe will provide a large surface area for the surface reactions, a high diffusion flux area and a shorter diffusion length, which is beneficial for a high growth rate. On the other hand, a small crystal size will result in a large saturation concentration of CNT, leading to a low driving force of carbon diffusion, and then a lower growth rate. A high surface reaction and low carbon diffusion will also lead to high surface carbon coverage, which will enhance the formation of encapsulating carbon via carbon polymerization. So the deactivation is also fast on the small particles [18]. The net effect of Fe crystal size on the rate of CNT formation is therefore a result of the competition among all the factors, and will result in an optimum size that will have the fastest growth rate. This optimum size effect has also been described recently [19].

The fact that the S–G (CA) catalyst yields a low growth rate clearly indicates that the increase in saturation concentration of CNT is dominating with the smallest particle size. This might explain why there is always a low productivity during single-walled carbon nanotube (SWNT) synthesis [20]. For SWNT synthesis, small catalyst particles are normally employed.

When the metal loading is increased without significant increase of the particle size (thus diffusion length), which is the case in this study, it is apparent that a large surface area for the surface reactions and diffusion flux exists. This will of course enhance CNT formation. However, if the metal loading is too high which will lead to very large particle sizes and consequently long diffusion length, then the growth rate

will be lowered. Hence it is envisaged that there is also an optimum metal loading that will bring the fastest growth rate, and this has been demonstrated by many researchers [21].

4. Conclusions

We have shown that the Fe particle size can be controlled through different catalyst preparation methods. Those catalysts have different properties, which are closely related to the formation of Fe_2SiO_4 and might have influence on the growth rate.

It was found that the CNT growth rate depends strongly on the catalyst particle size. An optimum particle size exists for the maximum growth rate, which has been demonstrated at two different temperatures. Therefore, small particle sizes do not necessarily lead to a high growth rate, and proper control of the catalyst particle size is critical for a high CNT production rate. Any parameters that have potential impact on the metal particle sizes, such as calcination or reduction process, might influence the growth rate. The growth rate also increases significantly with the metal loading. The growth process has been interpreted by a mathematical model, which explains the experimental results successfully. These findings have important practical meaning for the large scale synthesis processes.

Acknowledgment

The financial support from the Norwegian Research Council is gratefully acknowledged.

References

[1] P.M. Ajayan, Nature 427 (2004) 402.
[2] O.A. Nerushev, S. Dittmar, R.-E. Morjan, F. Rohmund, E.E.B. Campbell, J. Appl. Phys. 93 (2003) 4185.
[3] M. Yudasaka, R. Kikuchi, Y. Ohki, E. Ota, S. Yoshimura, Appl. Phys. Lett. 70 (1997) 1817.
[4] R.T.K. Baker, P.S. Harris, R.B. Thomas, R.J. Waite, J. Catal. 30 (1973) 86.
[5] P. Chitrapu, C.R.F. Lund, J.A. Tsamopoulos, Carbon 30 (1992) 285.
[6] C.L. Cheung, A. Kurtz, H. Park, C.M. Lieber, J. Phys. Chem. B 106 (2002) 2429.
[7] A.J. van Dillen, J.W. Geus, L.A.M. Hermans, J. van Der Meijden, in: Proceedings of the Sixth International Congress on Catalysis, vol. 2, 1977, pp. 677.
[8] J.W. Geus, N.V. Stamicarbon, US Patent 4,113,658 (1978).
[9] J.W. Geus, E. Boellaard, US Patent 5,143,877 (1992).
[10] R. Takahashi, S. Sato, T. Sodesawa, M. Kato, S. Takenaka, S. Yoshida, J. Catal. 204 (2001) 259.
[11] J.W. Geus, Appl. Catal. 25 (1986) 313.
[12] M. Perez-Cabero, I. Rodriguez-Ramos, A. Guerrero-Ruiz, J. Catal. 215 (2003) 305.
[13] M.A. Ermakova, D.Yu. Ermakov, A.L. Chuvilin, G.G. Kuvshinov, J. Catal. 201 (2001) 183.
[14] E. Rombi, I. Ferino, R. Monaci, C. Picciau, V. Solinas, R. Buzzoni, Appl. Catal. A 266 (2004) 73.
[15] R.T.K. Baker, J.J. Chludzinski, C.R.F. Lund, Carbon 25 (1987) 295.
[16] K.P. De Jong, J.W. Geus, Catal. Rev. -Sci. Eng. 42 (2000) 485.
[17] D. Chen, R. Lødeng, A. Anundskås, O. Olsvik, A. Holmen, Chem. Eng. Sci. 56 (2001) 1376.
[18] D. Chen, K.O. Christensen, E. Ochoa-Fernandez, Z. Yu, B. Tøtdal, N. Latorre, A. Monzón, A. Holmen, J. Catal. 229 (2004) 87.
[19] C. Ducati, I. Alexandrou, M. Chhowalla, G.A.J. Amaratunga, J. Robertson, J. Appl. Phys. 92 (2002) 3299.
[20] S.C. Lyu, B.C. Liu, S.H. Lee, C.Y. Park, H.K. Kang, C.W. Yang, C.J. Lee, J. Phys. Chem. B 108 (2004) 1613.
[21] S. Takenaka, S. Kobayashi, H. Ogihara, K. Otsuka, J. Catal. 217 (2003) 79.